Electrochimica Acta 426 (2022) 140800

Contents lists available at ScienceDirect

Electrochimica Acta

journal homepage: www.journals.elsevier.com/electrochimica-acta

Atomically-resolved structural changes of ceramic supported nanoparticulate oxygen evolution reaction Ir catalyst

Gorazd Koderman Podboršek [a,b,1], Ana Rebeka Kamšek [a,c,1], Anja Lončar [a,d,1,*], Marjan Bele [a], Luka Suhadolnik [e], Primož Jovanovič [a], Nejc Hodnik [a,b,d,*]

[a] Department of Materials Chemistry, National Institute of Chemistry, Hajdrihova 19, Ljubljana SI-1000, Slovenia
[b] Jožef Stefan International Postgraduate School, Jamova 39, Ljubljana SI-1000, Slovenia
[c] Faculty of Chemistry and Chemical Technology, University of Ljubljana, Večna pot 113, Ljubljana SI-1000, Slovenia
[d] University of Nova Gorica, Vipavska 13, Nova Gorica SI-5000, Slovenia
[e] Department for Nanostructured Materials, Jožef Stefan Institute, Jamova 39, Ljubljana SI-1000, Slovenia

ARTICLE INFO

Keywords:
Oxygen evolution reaction (OER)
Identical-location scanning transmission electron microscopy (IL-STEM)
Modified floating electrode (MFE)
Iridium nanoparticles
Titanium oxynitride support

ABSTRACT

The reduction of Ir loading and thus its efficient utilization in proton exchange membrane water electrolyzers (PEM-WE) inevitably depends on the rational design of novel nanomaterials. This, however, is not possible without the understanding of structure-stability interrelations and underlying mechanisms. When pursuing the reduction of Ir amount by its dispersion on ceramic materials, the interactions between the catalytically active sites and their support further complicate the already understood processes. In the present study, we use our unique approach, where we employ an Ir/TiON-based TEM grid and use it as a support system for the investigation of structural transformations of Ir nanoparticles. This was achieved by utilizing both the modified floating electrode (MFE) apparatus, which enables efficient bubble management during electrochemical experiments and identical-location scanning transmission electron microscopy (IL-STEM) approach. The analysis of obtained high-resolution images with in-house developed computer algorithms for image analysis reveals several processes with surface roughening being the predominant degradation mechanism. Additionally, suppressed oxidation tendency of supported Ir was directly confirmed.

1. Introduction

The larger-scale hydrogen production *via* water electrolysis is inevitably dependent on the reduction of the loading of a scarce iridium catalyst on the anode side of the electrolyzer, where an energetically expensive oxygen evolution reaction (OER) takes place. Together with efficient iridium recycling, it is recognized as one of the grand challenges on the way to overcome the barriers of proton exchange membrane water electrolyzer (PEM-WE) market maturation [1]. However, the decrease in loading of pure Ir catalyst can lead to deterioration in performance, specifically due to a reduction in thickness of the catalytic layer and thus its lower homogeneity. Ideally, the thickness of the anode layer with Ir loading 0.5 mg cm^{-2} should be between 4 and 8 μm [2].

This target could be achieved by introducing highly conductive and stable supports for Ir-based nanoparticles, similarly to Pt catalysts in fuel cells, which are typically supported on carbon-based high surface area materials [3]. The use of carbon supports for OER catalysts is however limited, due to its thermodynamic instability at high anodic potentials. Instead, different oxides are often considered in the literature, namely tin oxide and its doped analogues [4–6], titanium oxide [7,8], its suboxides [9], or titanium oxynitride TiON [10]. While each of the studied materials showed promising results on the laboratory scale, it needs to be noted that especially their long-term stability should be critically addressed in future studies to justify their use in PEM-WE [11,12]. Compared to carbon, ceramic supports have at least one strong advantage, namely, their electrochemical oxidation does not irreversibly affect active sites due to the collapse of its structure. Thus, ideally, the structure and the thickness of the catalyst layer should remain intact [13,14]. Not only does ceramic support enable efficient dispersion and anchoring of the active nanoparticles, but can also enhance the catalytic properties of the active material *via* metal-support interactions. This phenomenon, well known in the field of heterogeneous catalysis [15–19], is getting

* Corresponding authors.
E-mail addresses: anja.loncar@ki.si (A. Lončar), nejc.hodnik@ki.si (N. Hodnik).
[1] Authors contributed equally.

https://doi.org/10.1016/j.electacta.2022.140800
Received 16 February 2022; Received in revised form 30 June 2022; Accepted 2 July 2022
Available online 4 July 2022

recognition also in OER electrocatalysis [20,21]. When comparing Ir nanoparticles, supported on TiON or carbon, Bele et al. observed lower oxidation of Ir supported on ceramic material *via* cyclic voltammetry [10]. Using near-ambient pressure X-ray photoemission spectroscopy (NAP-XPS), complemented with downstream analytics, Saveleva et al. similarly revealed that, compared to the unsupported catalyst, SnO_2:Sb-supported metallic Ir nanoparticles show a significantly lower tendency to oxidize [22]. Concretely, XPS spectra of supported particles at 1.7 V are dominated by the metallic features with only minor contributions from Ir^{4+} and Ir^{3+} species, which are generally assumed to be the unstable intermediate in OER, leading to a higher dissolution of active Ir-based electrocatalysts [23]. The enhanced stability was explained by the oxygen spill-over mechanism from Ir to the SnO_2:Sb, resulting in the observed formation of a thinner oxide layer on the surface of supported nanoparticles, which was also in agreement with the detected lower dissolution rate.

This behavior suggests the ongoing structural changes, which were however not observed with *ex-situ* (scanning) transmission electron microscopy ((S)TEM) analysis of the sample before and after the experiment [23]. Nevertheless, to thoroughly understand the strong metal-support interaction (SMSI) effect and correlate it to the structure-stability mechanistic interrelation, a more detailed study would be of relevance. Especially since observing random locations at relatively low magnifications, as typically done, cannot distinguish between the reaction-induced nanoscopic changes, occurring on a specific site or features that were there prior to electrochemical operation. Such a limitation can be elegantly solved by employing the identical location (IL-TEM) approach, which is now generally well established in the field of electrocatalysis [24,25]. Its utilization allows us to observe structural, morphological, and compositional changes of individual nanoparticles before and after the reaction. This is instrumental if we want to understand the real nature of nanoparticulate electrocatalysts and their effect on the catalytic properties, which is often far more complicated than the theoretical predictions, commonly based on perfectly shaped particles [26,27].

Besides the high-resolution STEM imaging, the study of degradation processes with IL-TEM also depends on the rational design and performance of electrochemical experiments and objective interpretation of the obtained micrographs. Firstly, performing electrochemical and microscopical experiments on the same specimen is challenging, especially since TEM analysis requires a very thin catalyst layer, deposited on the fragile TEM grid. Aiming to resolve the low-loading issue, a novel methodological approach, namely modified floating electrode (MFE) was recently presented and showcased on the oxygen reduction reaction (ORR) [28]. Here, an Au TEM grid with a deposited Pt-based catalyst layer was used as a working electrode, floating on the surface of the electrolyte. Furthermore, MFE resolves the challenge related to the mass transport in the ORR measurements, as here the reactant can be delivered directly to the catalyst layer and thus allows reaching realistic current densities. In the case of OER electrocatalysis, this is however not so trivial, as the gas is not consumed but rather produced. Due to the low solubility of oxygen molecules in the electrolyte, gas bubbles stay trapped in the catalytic layer and block the active surface area of the catalyst [29]. This is especially problematic during stability measurements, as it can lead to misinterpretation of the electrochemical results [30,31].

Secondly, the accurate interpretation of the data obtained *via* microscopy is essential for understanding degradation mechanisms. To get insight into how a single nanoparticle changes during the experiment, the images before and after an electrochemical treatment must be compared. Pursuing structural changes at the atomic level is not only time-consuming but can also be to some degree subjective. Thus, the development of computer algorithms for image analysis would be highly beneficial for spotting differences [27]. While their implementation was already showcased for ORR catalysts [32], OER catalysts have, to the best of our knowledge, still not been investigated by this approach.

This work aims to reveal the structural changes of TiON supported Ir nanoparticles of different sizes during the OER through a unique methodology enabling grid-based synthesis, electrochemical measurements, and identical location imaging supplemented by automated image analysis. Initially, we show that efficient bubble management during the prolonged stability measurement is achievable with a dynamic protocol, consisting of open circuit potential (OCP) and OER intervals, which is a prerequisite for further investigation. To understand the effect of the interactions between Ir and TiON on the oxidation tendency and dissolution of Ir nanoparticles, we use a combination of MFE-IL-STEM analysis and in-house developed computer algorithms for subsequent analysis of IL-STEM images, which reveal several structural changes at the atomic scale. The acquired knowledge will not only accelerate the development of novel materials with enhanced electrocatalytic properties but will also contribute to the emergence of innovative recycling techniques. This is essential, as they will enable the recovery of iridium and other platinum group metals (PGM), initially produced *via* extremely energy-demanding and polluting processes [33–35].

2. Experimental

2.1. Sample preparation

The investigated sample is based on the novel experimental approach, which aims to synthesize and characterize the catalyst on the same TEM grid. The main advantage of this unique platform is the ability to track nanoscale events on the identical location occurring during the synthesis and electrochemical investigation. The synthetic procedure, which was already shown to be a viable approach for the synthesis of OER catalysts [21,36] and was here accordingly adjusted for exploitation on a TEM grid, consisted of TiON preparation and deposition of Ir nanoparticles. TiON grid was prepared by potentiostatic anodization (40 V, 30 min) of Ti TEM grid (3.05 mm diameter, 100 mesh, SPI Supplies). This was done in a two-electrode configuration with a stainless-steel counter electrode and an anodization electrolyte consisting of 0.3 wt. % NH_4F (99.99%, Sigma-Aldrich) and 2 vol.% deionized water in ethylene glycol (99.5%, Carlo Erba Reagents). The Ti grid was immobilized and electrically wired with a specifically developed sample holder. The anodization resulted in an amorphous TiO_2 nanotube micrometer-thick film, which was transformed into crystalline TiO_2 nanotubes by annealing at 450°C (heating and cooling rate of 5°C min^{-1}) for 1 hour in air. The grid was afterward annealed at 730°C (heating and cooling rate of 5°C min^{-1}) for 2 h in an ammonia atmosphere to convert TiO_2 to TiON substrate with an increased surface area compared to the initial Ti grid. The flow of pure ammonia gas was kept constant at 50 cm^3 min^{-1} and a pressure of 1 atmosphere. In the next step, Ir nanoparticles were deposited by dipping the grid halfway in the water solution of iridium (III) bromide hydrate (Sigma-Aldrich, St. Louis, MO) with a concentration 20 mg ml^{-1} (withdrawal rate 1 cm s^{-1}) and dried at 50°C. The sample was then thermally treated at 700°C (fast heating and cooling rate of 100°C min^{-1}) for 15 min in a 5 % H_2/Ar atmosphere.

2.2. Electrochemical characterization

For electrochemical experiments, a modified floating electrode (MFE) apparatus was used in an H-cell setup with compartments, separated by a Nafion membrane (Nafion 117, FuelCellStore) (Schematic presentation in SI - Scheme S1). MFE apparatus was assembled from a two-piece Teflon housing, a metallic spring, placed between two metallic cones, a gas diffusion layer (GDL, 280 μm thickness) with 40% Teflon weight wet proofing (Toray Carbon Paper 090, Fuel CellStore) and the homemade Ir/TiON TEM grid, used as the working electrode. A reversible hydrogen electrode (HydroFlex®) and a Pt mesh were used as reference and counter electrodes, respectively. The counter electrode

was placed in a separate compartment to prevent any possible Pt contamination on the TEM grid. A freshly prepared 0.1 M perchloric acid ($HClO_4$, 70% Rotipuran Supra, Carl Roth, diluted by Milli-Q, 18.2 Ω cm) was used as an electrolyte. A gas tube was inserted in the holes in the Teflon housing of MFE to purge the system with inert Ar. The grid was initially imaged with STEM to record the as-synthesized state of the catalyst. Then, the electrochemical protocol consisted first of potentiostatic hold at 1.6 V for 30 minutes. Before and after this step, catalyst activity was measured with 3 consecutive cycles between 1.2 and 1.6 V with a scan rate of 10 mV/s. Afterward, structural characterization with STEM was performed. The following electrochemical experiment consisted of 3 cycles of the "dynamic degradation protocol." Each cycle consisted of 60 repetitions of intervals at 5 mA cm^{-2} (30 s) and 0 mA cm^{-2} (45 s). After each cycle, the system was purged with Ar at OCP for 10 min, and then 20 cyclic voltammograms between 0.05 and 1.45 V with a scan rate 300 mV/s were recorded to follow the structural changes of Ir. Activity before and after the "dynamic degradation protocol" was evaluated as above. Schematic presentation of the experimental protocol is provided in SI - Scheme S2. During all experiments, 85% Ohmic drop compensation was applied. Finally, structural characterization with STEM was again performed.

2.3. Structural characterization – scanning transmission electron microscopy

IL-STEM imaging was performed in a Cs-corrected transmission electron microscope (CF-ARM Jeol 200) equipped with an SSD JEOL EDX spectrometer and a GATAN Quantum ER dual-electron energy loss spectroscopy (EELS) spectrometer. An operational voltage of 80 kV was employed. The images were taken in STEM mode (bright-field, BF and high angle annular dark-field, HAADF), probe size 6C, 8 cm effective camera length.

2.4. Image processing algorithms

Atomically resolved identical location STEM images were analyzed using in-house image processing algorithms. Positions of atomic columns were determined *via* a two-step process. First, their initial approximations were established by pre-processing the images and calculating centers of mass for intensity distributions of all columns. Second, approximate column positions were refined by fitting 2D asymmetric Gaussian distributions onto intensity values in the close vicinities of previously determined approximate positions of atomic columns. Refined positions were determined as centers of the fitted 2D asymmetric Gaussian distributions. Atomic-scale surface roughness of nanoparticles was assessed by nearest neighbor analysis. For each atomic column, its neighboring columns were determined based on their proximity to the column in question. Atomic columns were then marked with different colors depending on their number of nearest neighbors. Finally, the particle size distribution was performed using an in-house segmentation algorithm based on adaptive thresholding. Anomalies were corrected manually. All code was written in Python programming language using open-source libraries.

3. Results and discussion

The investigation started with the STEM structural characterization of the Ir/TiON grid, which serves as a model system for a deeper understanding of the structure-stability relationship of Ir electrocatalysts. In Fig. 1, STEM images of the Ir/TiON grid after the Ir deposition at low magnification are shown. The nanotubular morphology can be recognized by the approximately 40 nm circular openings on the bottom left images. Ir nanoparticles are seen as contrasting spots in sizes up to 15 nm. Due to a specifically selected temperature program (fast heating, i.e. 100°C min^{-1}) during iridium bromide reduction, the Ir nanoparticle size has a wide distribution (Fig. S1) and additionally, twin boundaries are often observed in the nanoparticles (Fig. 1). With the usual Ir nanoparticle deposition method (wet impregnation, slow heating, i.e. 2°C min^{-1}, 1 h at 400 (450)°C), the formed Ir nanoparticles tend to be very small (1-2 nm diameter) as a result of the dried $IrBr_3$ nanocrystals reduction and coalescence [21]. However, once formed, these small Ir nanoparticles are very stable and further heating does not cause any further particle growth. In our previous investigations, the Ir nanoparticles were too small to see changes on individual crystal facets, therefore we aimed to obtain bigger nanoparticles for this study. Fast heating and a high-temperature treatment of dried $IrBr_3$ nanocrystals were chosen, as faster heating to higher temperatures causes the formation of nanoparticles with wider size distribution and with more

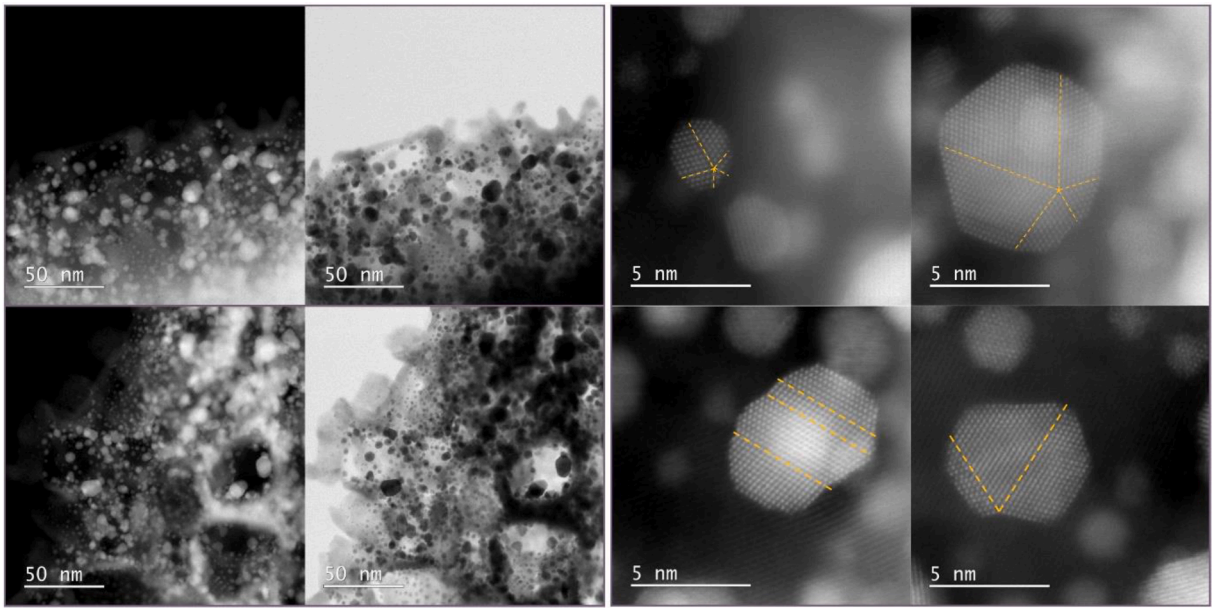

Fig. 1. Bright-field (BF) and high angle annular dark-field (HAADF) images of the as-synthesized Ir/TiON grid at low magnification (left). Cyclic and polysynthetic twinning, observed in Ir nanoparticles of different sizes (right). Twin boundaries are depicted with orange dashed lines. (For interpretation of the references to color in this figure legend, the reader is referred to the web version of this article.)

defects. As we observed that the largest Ir nanoparticles are being formed on the edge of the solution and the middle of the grid is the optimal location for TEM imaging, only half of the grid was dipped in the $IrBr_3$ solution for practical reasons.

After the structural analysis of the as-prepared grid and selection of nanoparticles with different sizes for IL-TEM spots, the first electrochemical experiment, i.e. potentiostatic activation was performed. This step was included to **i)** test if long-term stationary protocols are suitable for the use in MFE for OER studies and **ii)** to oxidize the support and Ir nanoparticles before evaluation of the electrochemical activity. This is relevant, as simultaneous oxidation events, i.e. Faradaic contributions of TiON and Ir oxidation with an excursion to high anodic potentials, can affect the interpretation of the measured OER current (discussion on TiON oxidation is given in SI, Fig. S2) [21,37]. In Fig. 2a, activity before and after the 30 min polarization at 1.6 V is shown. In this study, we normalized the current by the geometric surface area of the grid that is in contact with the electrolyte, defined by the opening in the Teflon housing, as the exact mass and surface area of Ir are unknown. The edge of the grid, also containing a portion of deposited Ir, due to the specific synthetic procedure, is partially covered by the Teflon housing. The exact mass of Ir nanoparticles that are in contact with the electrolyte is thus unknown, which would make normalization by Ir mass meaningless. The most appropriate would be the evaluation of the intrinsic activity by active surface area (ECSA) normalization, however, there is currently no suitable method for reliable and comparable estimation of the ECSA of supported oxide materials, despite some promising attempts [38,39]. For a rough estimation of the surface area of metallic nanoparticles H_{upd} charge and for oxidic materials voltammetric charge of the $Ir^{3+/4+}$ transition are often used [40]. Nevertheless, in our case, both features are present even after degradation. As there is, to the best of our knowledge, no measure to evaluate the proportion of each phase, and using just one of them would also be incorrect, it would be unreliable to attempt such current normalization to evaluate the intrinsic properties of the investigated material. Nevertheless, the normalization by geometric surface area allows a qualitative analysis of the obtained data, giving information about electrocatalytic and structural changes of the catalyst during the electrochemical biasing. As a result of the electrochemical oxidation of Ir, the measured current after activation is, as expected, higher due to the formation of a thin Ir oxide, which is known to have higher intrinsic activity than non-activated metallic Ir [41].

To overcome the problems, related to bubble accumulation during stationary experiments, we designed a dynamic degradation experiment, similar to the protocols used in the literature [42,43]. Based on the conclusions from experiments during the protocol development, which is in more detail discussed in SI (Figs. S3 and S4), we performed the degradation experiment on the Ir/TiON grid with 30 and 45 s long "start-stop" intervals at 5 mA cm^{-2} and OCP, respectively. The results are shown in Fig. 2b. In combination with Ar purging, this protocol is efficiently removing the produced gas molecules. This is one of the crucial aspects in OER catalysis which, however, is only rarely taken into account.

The first indicator of structural changes on Ir during the degradation experiment are cyclic voltammograms, shown in Fig. 2c. After each cycle of the dynamic protocol, 20 fast CVs were recorded in a broad potential range (0.05 – 1.45 V). At the beginning of the protocol, at least some portion of Ir is still in a metallic state, confirmed by the characteristic H_{upd} feature between 0.05 and 0.35 V [44]. Interestingly, this peak is present throughout the experiment, which indicates that Ir has indeed a lower tendency to oxidize when it is supported on the ceramic material, which is in agreement with the study by Savinova et al. [22] and Bele et al. [10]. Still, the appearance of another broad Ir feature at approximately 0.9 V, characteristic for Ir^{3+} to Ir^{4+} transition, indicates that nanoparticles are getting oxidized at least to some extent during the experiment. The second indicator of structural changes is also the increased activity of Ir nanoparticles after the dynamic degradation protocol, which goes in line with the literature reports [45].

To deepen the insights into the structural changes after the two respective electrochemical steps, IL-STEM imaging of the sample at different magnifications was performed (Fig. S5). Most importantly, five nanoparticles that remained in the zone axis during all three STEM

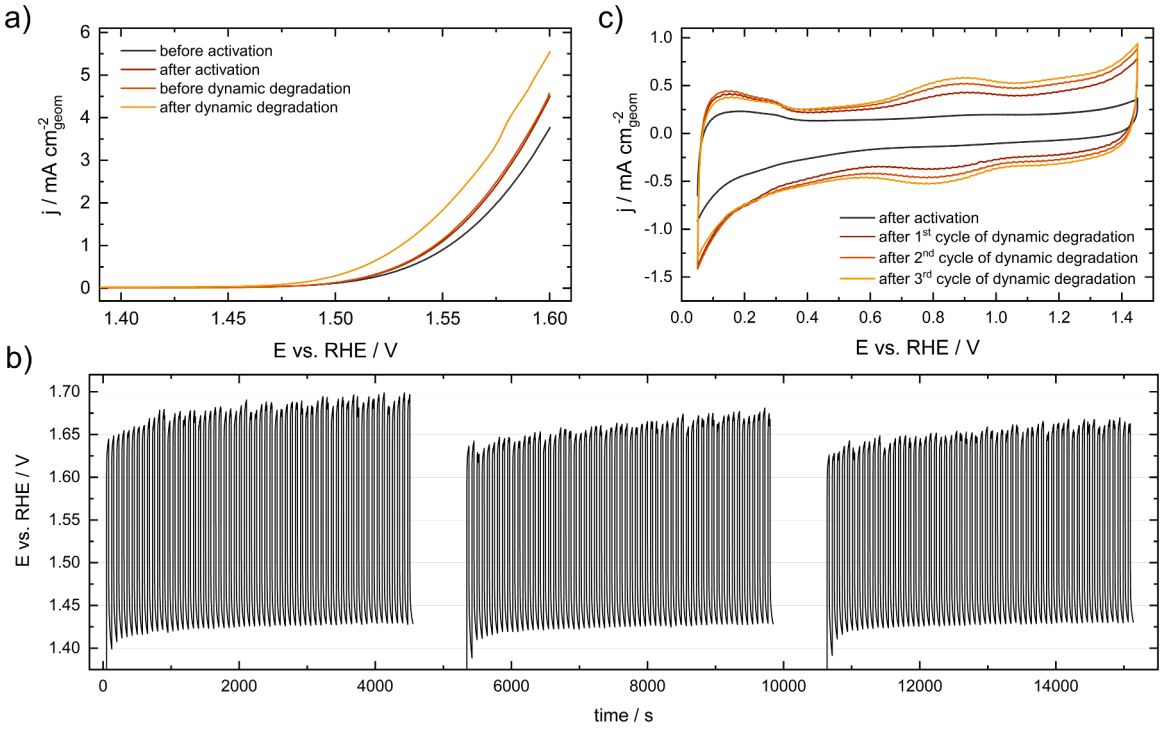

Fig. 2. (a) OER polarization curves for activity evaluation before and after the potentiostatic activation protocol, and before and after the dynamic degradation protocol, (b) dynamic degradation protocol, the minor increase in potential indicates successful bubble management while the decrease in potential during the experiment indicates the formation of a more active catalytic phase, (c) evaluation of structural changes of metallic Ir during the electrochemical degradation.

imaging steps were taken at atomic resolution and analyzed with in-house developed image analysis algorithms. In Figs. 3 and 4, IL images of two Ir nanoparticles are shown in the as-synthesized state, after activation, and after dynamic degradation. Along with original STEM images, positions of the atomic columns are shown in blue for each step of the process. The reader can find the identical location images of the remaining nanoparticles in the SI (Fig. S5 for images at a lower magnification and for nanoparticles outside of the zone axis, and Figs. S6–S8 for the three remaining nanoparticles, imaged at atomic resolution).

Identical location images of the sample at a lower magnification and of nanoparticles, which did not stay in the zone axis during the entire experiment, do not reveal any large-scale restructuring of the Ir nanoparticles or the TiON support during the electrochemical perturbation. They do, however, show that individual nanoparticles migrate across the support, that their surface is getting rougher, and that some degree of amorphization at their surface can be observed. Such data provides general information about a more statistically relevant number of nanoparticles, which unfortunately lacks atomically resolved insights that can be easily quantified. Therefore, our efforts focus on quantifying the information available in sets of atomically resolved identical location images, which provides more accurate results about the structural changes at the atomic level.

Before the analysis of the structural evolution of the investigated nanoparticles, a brief overview of the state-of-the-art understanding of the restructuring and oxidation of single-crystalline and nanoparticulate materials is given. In general, the structure-stability interrelations are relatively poorly understood. Özer et al. showed in their single-crystal work that the surface orientation importantly influences the formation of the oxide layer, i.e. more open planes of Ir (110) are more prone to oxidation than Ir (111). Additionally, the morphology of the oxide, grown either on opened or closed, denser planes is different [46]. Similar conclusions on the rate of oxidation of opened surfaces were obtained in a study by Scohy et al [47]. Here, the authors studied both single crystalline and nanostructured surfaces. They concluded that the original structure and chemical composition initially influence the growth of the oxide, however, all surfaces gradually transform into a similar phase. By combining dissolution measurements with XPS, they discovered that after a two-hour polarization at a higher anodic potential, the dissolution is accompanied by the increase of the metallic Ir peak, which was attributed to the thinning of the formed oxide on the surface of the underlying metal. The recent study by BalaKrishnan et al. combined atom probe tomography (APT) with XPS to probe the structural transformations of the needle-shaped Ir probe [48]. Here, the authors concluded that the formation of the oxide phase depends on the nature of planes. While on the closed planes (e.g., (111)) the growth of the oxide layer stops at 1 – 2 nm, the growth of the subsurface oxide phase on opened planes, containing metastable Ir-O species, continues to approximately 10 nm thickness after 300 s at 1.55 V. This affects the catalytic activity of different crystallographic planes. Their results suggest that the formation of a “sandwich structure” of oxide, generally assumed in the literature of hydrous iridium oxide [49,50], is limited only to open planes.

None of the mentioned works though included supported Ir nanostructures in the investigation. Thus, we continue the discussion on the understanding of the surface orientation dependence on the reactivity and degradation mechanisms with our IL-STEM results obtained on Ir/TiON. Inspecting the five different nanoparticles, we can conclude that only minor changes occur during potentiostatic activation. Even though slow oxidation might be the reason for this conclusion according to the CVs, we cannot completely eliminate the possibility that particles were partially blocked by generated gas bubbles. As all five recorded nanoparticles were imaged in the same zone axis, namely [110], it is also possible that the changes occurred in the direction(s) we did not systematically observe. The transformation of the nanoparticle surface for the five nanoparticles in the [110] zone axis is, however, clearly observable after the longer dynamic degradation. Surface roughening, i.e. losing the faceted shape is the predominant phenomenon, observed in the images. This seems to be independent of the surface orientation, in contrast with the reports in the literature, discussed above. Instead, changes to the nanoparticle surface seem to be induced at the edges of individual facets, while columns in the middle of a well-defined crystal facet seem to be exempt from change. Additionally, we observed a few localized changes that could be ascribed to amorphous growths occurring predominantly on {001} facets and, to a lesser extent, on {111} facets which somewhat confirm previous findings about {111} planes

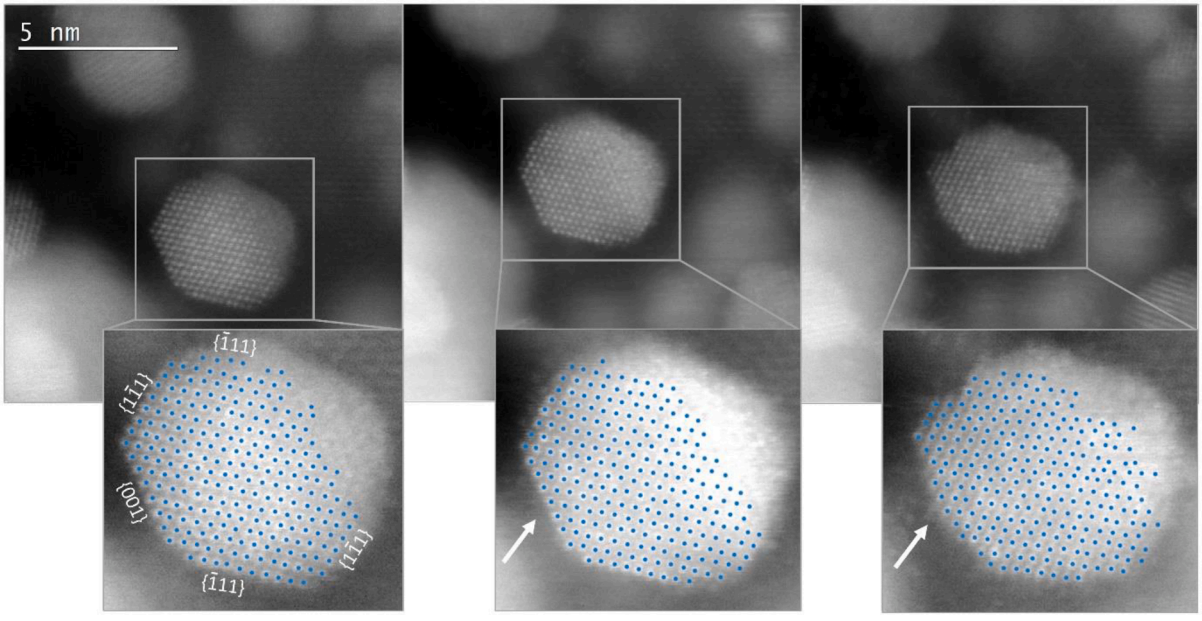

Fig. 3. IL-STEM images of a smaller Ir nanoparticle, from left to right: before electrochemical biasing, after potentiostatic activation, and after dynamic degradation. Top: original STEM images, bottom: enhanced contrast images with overlaid positions of atomic columns in blue. The white arrow signifies the site with observed potential amorphous growth after dynamic degradation. (For interpretation of the references to color in this figure legend, the reader is referred to the web version of this article.)

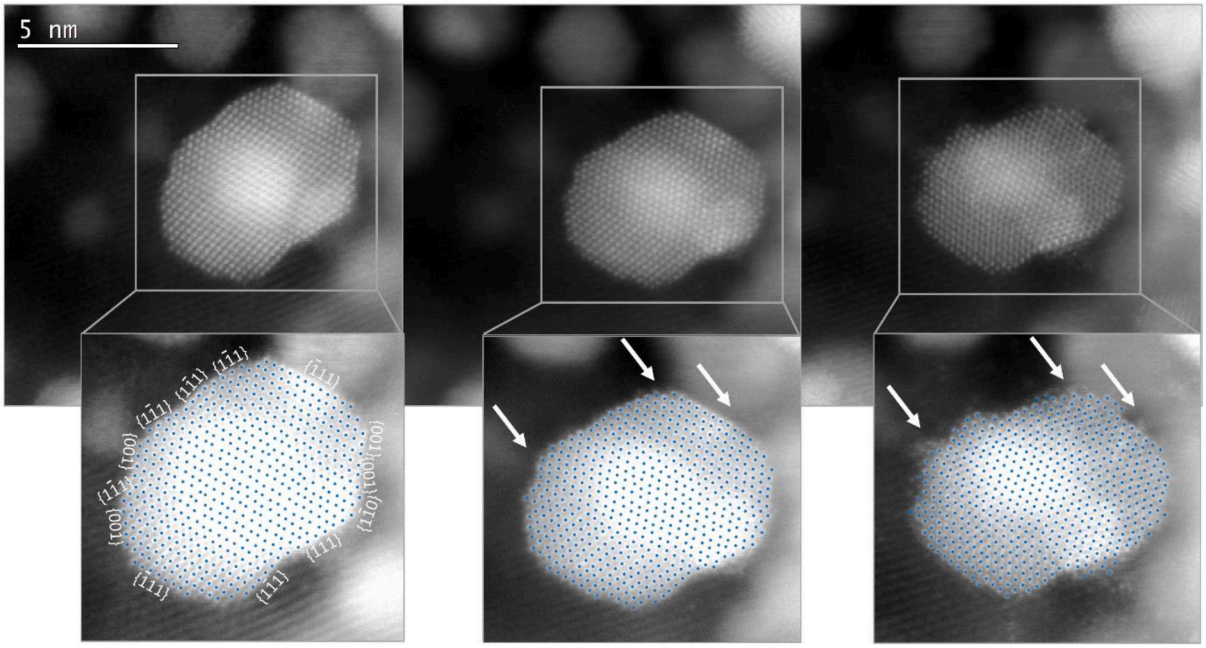

Fig. 4. IL-STEM images of a larger twinned Ir nanoparticle, from left to right: before electrochemical biasing, after potentiostatic activation, and after dynamic degradation. Top: original STEM images, bottom: enhanced contrast images with overlaid positions of atomic columns in blue. White arrows signify the sites with observed potential amorphous growth after dynamic degradation. (For interpretation of the references to color in this figure legend, the reader is referred to the web version of this article.)

being less favorable for oxide layer growth [46–48] but cannot be quantified with certainty due to the low number of occurrences of such growth. Again, we emphasize that we cannot comment on possible dissolution and oxidation of other surface crystal planes as they are not frequently present on the edges of the studied nanoparticles. This kind of comprehensive information about the possible correlations between facets and observed changes would only be accessible by expanding our approach with electron tomography and 3D reconstruction algorithms or by imaging a larger ensemble of hundreds of nanoparticles, which is currently not feasible in our laboratory.

To statistically evaluate the proportion of surface roughening, we classified the registered atomic columns by the number of their nearest neighbors (Fig. S9). By doing this, we aimed to understand the process of surface roughening on the nanoparticle during OER. In Fig. 5 (the rest of the nanoparticles in Fig. S10), the two nanoparticles already depicted above are represented with circles for positions of their atomic columns, colored by the number of their nearest neighbors. In the two-dimensional projection of the nanoparticle with a face-centered cubic structure, each atomic column can have up to 6 nearest neighbors. Atomic columns, found in the interior, have 6 nearest neighbors, while columns on the nanoparticle surface have an array of different numbers of nearest neighbors. Here, it is important to point out that some of the

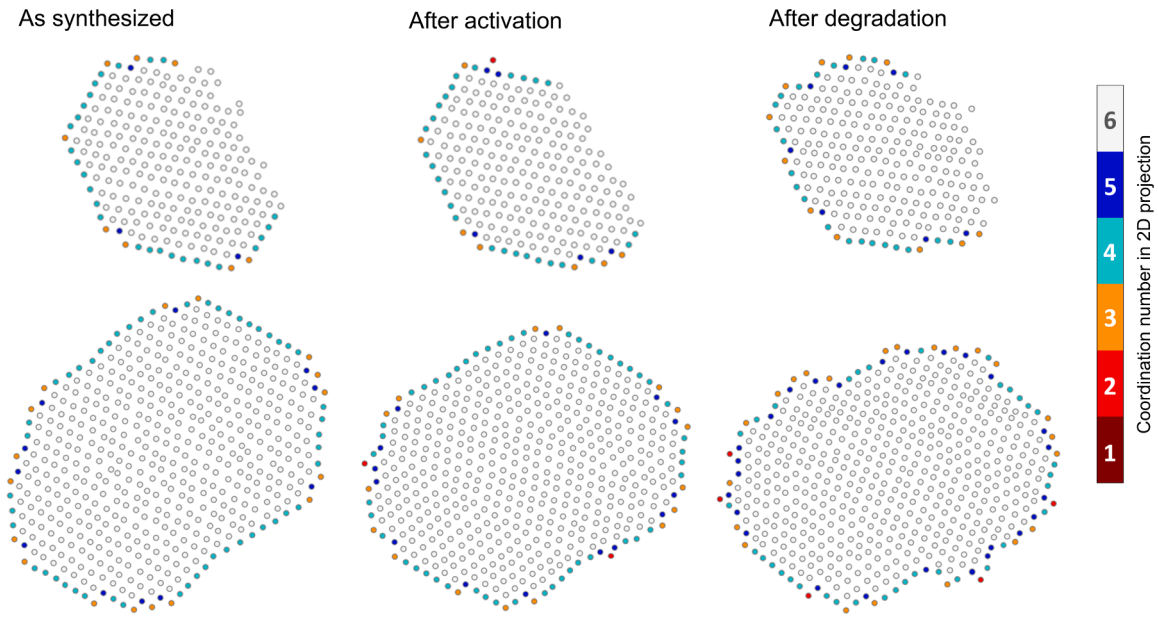

Fig. 5. Visual presentation of the atomic columns with different numbers of nearest neighbors on two individual nanoparticles. Legend: 6 neighbors – interior columns, 5 neighbors – surface columns in concave sites, 4- neighbors – part of a well-defined facet, 2 or 3 neighbors – edges of facets.

nanoparticles, for example, the one in Fig. 3, are twinned in such a way that only one part of the nanoparticle is imaged at atomic resolution while the other part is not in the zone axis. In such cases, we excluded the atomic columns next to the grain boundary from analysis as there is no way of knowing how many nearest neighbors they truly have. Since we are exploring the surface roughening phenomenon, observed in STEM images, we are interested the most in the change of the share of atomic columns with a specific number of nearest neighbors by different steps of the electrochemical protocol.

The share of columns with a specified number of nearest neighbors was calculated for each of the five nanoparticles (Fig. 6). In these graphs, the nanoparticle depicted in Fig. 3 is labeled as "particle no. 2" and the nanoparticle in Fig. 4 is labeled as "particle no. 5". We focused on tracking the changes to the share of columns with 4 nearest neighbors for all five imaged nanoparticles to show the loss of a faceted shape, and on tracking the changes to the share of columns with 2, 3 or 5 nearest neighbors to similarly show how the surface is getting rougher at the atomic scale. There were no columns found with only one nearest neighbor. The analysis of nearest neighbors confirmed that the number of the sites located on a facet indeed decreases during dynamic degradation, while the number of defects, i.e. edges, steps, and kinks increases. Only one of the nanoparticles did not follow this trend, in Fig. 6 labeled as "particle no. 1". This is the smallest of all studied nanoparticles and thus exhibited a noticeably larger ratio of surface atomic columns to interior atomic columns. However, this nanoparticle also exhibited evident reshaping during both electrochemical protocols (Fig. S6). Interestingly, these dynamic changes did not result in a roughening. This can be explained by the fact that the original small nanoparticle already has a high share of columns with 2, 3 or 5 nearest neighbors and any further surface atom movements do not increase this ratio. Thus, we can conclude that small nanoparticles with facets made out of 3 to 5 atomic columns and a high ratio of surface atomic columns to interior atomic columns can not be further roughened. Close inspection of Fig. S6 reveals the dynamic interplay of surface planes which is probably changing back and forth into the same shapes. Based on this, we can conclude that noticeable surface roughening of Ir nanoparticles above approximately 3 nm in diameter takes place during dynamic degradation. Below this size, the surface does not roughen further but still exhibits noticeable dynamic changes. As the smaller nanoparticles of Ir are desired to enhance its utilization in PEM-WE, their stability is critical. It was recently shown by DFT, that the adhesion of nanoparticles to the surface of TiON is stronger for smaller particles, which suggests their improved stability [21]. Interestingly, when comparing charge-normalized dissolution of two samples with different Ir particle size distributions, a lower dissolution tendency of smaller particles was observed [51].

While the image analysis of Ir nanoparticles before and after electrochemical perturbation identified surface roughening as the predominant degradation mechanism, it is important to consider the possibility of multiple processes taking place at the same time. To quantify the loss of Ir atoms of a single nanoparticle due to dissolution, it would be ideal to count down the number of atoms in particles of different sizes based on the HAADF intensity in STEM images. If unsupported particles were studied, this would be possible with our approach, however, we were not able to eliminate the signal of the ceramic support on the images yet. Nevertheless, based on the qualitative analysis of the images, the overall number of columns, comprising each nanoparticle, did not change significantly during the experiment, hence we can conclude that no substantial dissolution took place. Considering the fact that dissolution can influence the onset of other mechanisms, there is a possibility that some minor dissolution occurs, followed by redeposition of the dissolved atoms at different surface sites. However, an alternative explanation for the observed surface roughening is surface diffusion. To determine exactly what happened during the experiment, liquid cell transmission electron microscopy should be performed, although using this technique would most likely mean a compromised spatial resolution and losing the ability to observe the changes on a column-to-column basis.

While oxide features, appearing in the CVs after dynamic degradation protocol indicate that the surface of the investigated nanoparticles must be at least to some degree oxidized, the IL-HAADF-STEM images only showed a few localized occurrences of potential amorphous growth. These observations confirm previous studies, which showed that supported Ir nanoparticles are stabilized by SMSI through a lower oxidation tendency compared to the unsupported Ir [10,22]. Interestingly, the effect of different support on the amorphization is clearly seen on the IL-TEM images in our recent study, where we compared two materials with Ir supported on TiON/C matrix [51]. Here, presence of carbon seems to enhance the reshaping of nanoparticles to significantly higher degree. To eliminate the possibility of overlooking the oxide layer due to contrast-related limitations, we overlaid the atomic columns in the particles before and after electrochemical perturbation to detect the potential changes in the crystal lattice due to oxidation after the degradation (Fig. S11). The results were, however, not conclusive due to technical limitations of STEM imaging and the nature of the sample and the experiment. During the electrochemical degradation, the TEM grid wrinkles, which causes slight tilts away from the zone axis of the chosen Ir nanoparticles. Additionally, the Ir particles and local changes of the TiON support during electrochemical degradation and under the TEM electron beam are also too small to correct the tilt via tilting the holder (no Kikuchi lines to determine the necessary tilting direction), which leads to elongated projections of atomic columns. Together with potential small drifts during STEM imaging, it is not possible to perfectly overlap the atomic columns of images before and after degradation. All these effects might hide signs of an oxide layer. Elemental analysis with EELS or EDXS was also considered, but the idea was discarded as the results would be inconclusive as well due to the irregularly distributed oxygen in the TiON support and to avoid any potential beam damage.

Nevertheless, the surface changes seem to be orientation

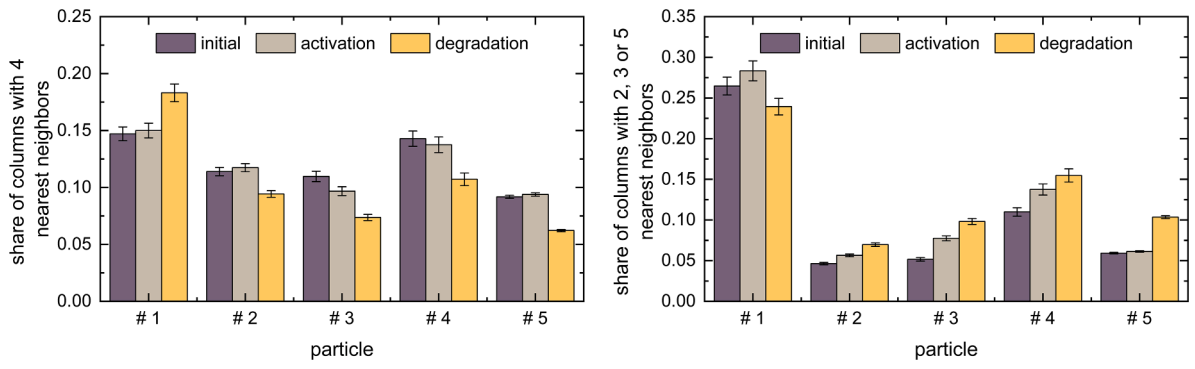

Fig. 6. Graphical representation of the share of columns with 4 neighbors (part of a well-defined facet; left) or 2, 3 (edges of facets) or 5 (columns in concave sites) nearest neighbors (right).

independent, in contrast to the literature reports discussed above, which could be explained by the particle size effects and the inevitable presence of surface defects in nanoparticles. This conclusion is similar to observations of intermetallic Pt alloys, used as ORR catalysts [32]. The study by Saveleva et al. additionally suggested that the stabilization of Ir via oxygen spill-over mechanism could be balanced by the partial encapsulation of the Ir nanoparticles with a layer of SbO_2, which was based on the increased Sn/Ir ratio. The IL-STEM images revealed a minor presence of an amorphous phase on the surface, which could be in favor of this suggestion, however, currently, it is not possible to confirm whether it is the formation of Ti or Ir oxide on the surface of nanoparticles. To confirm this hypothesis on SMSI stabilization mechanisms, one should also thoroughly inspect the changes of the support, which will be the scope of our future investigations.

4. Conclusion

In conclusion, the presented study aimed to reveal the structural changes of Ir nanoparticles during OER, by employing a novel approach, which allows studying nanoscale events during the synthesis and electrochemical biasing with STEM on a single TEM grid. We used the Ir/TiON model system, which was prepared by anodization of Ti TEM grid, its transformation into TiON *via* annealing in ammonia atmosphere and subsequent deposition of metallic Ir nanoparticles. The electrochemical investigation was done in an MFE apparatus, which, together with an innovative dynamic degradation protocol, enabled a sufficiently long degradation experiment without possible bubble-accumulation-driven limitations. Structural analysis, done with IL-STEM and in-house developed algorithms for atomically-resolved image analysis, revealed a low oxidation tendency of metallic Ir nanoparticles and surface roughening as the predominant degradation mechanism by tracking the share of atomic columns with a specified number of nearest neighbors. Particles, larger than 2 nanometers in diameter, exhibited an increase in the number of surface defects such as steps and edges, while a smaller investigated nanoparticle only exhibited some restructuring. The surface roughening influenced the electrocatalytic properties of initial particles, namely, it increased the activity after the dynamic degradation protocol. Our novel approach gave us insight into the atomically-resolved dynamic behavior of nanoparticulate OER catalysts, which will deepen the understanding of the structure-stability relationship and guide the design of novel catalysts with superior catalytic properties. Nevertheless, to avoid possible limitations of STEM that requires a high vacuum, the structural analysis should be in the future complemented with complementary in-situ techniques, such as Raman spectroscopy [52,53].

CRediT authorship contribution statement

Gorazd Koderman Podboršek: Conceptualization, Methodology, Investigation, Data curation, Writing – review & editing. **Ana Rebeka Kamšek:** Methodology, Software, Formal analysis, Investigation, Data curation, Writing – original draft, Writing – review & editing, Visualization. **Anja Lončar:** Conceptualization, Methodology, Validation, Investigation, Data curation, Writing – original draft, Writing – review & editing, Visualization. **Marjan Bele:** Resources, Methodology, Investigation. **Luka Suhadolnik:** Resources, Methodology, Investigation. **Primož Jovanovič:** Writing – review & editing, Funding acquisition. **Nejc Hodnik:** Conceptualization, Supervision, Funding acquisition.

Declaration of Competing Interest

The authors declare no conflict of interest.

Acknowledgments

Authors gratefully acknowledge prof. dr. Goran Dražić for his valuable comments and fruitful discussions about the subject of this work and Armin Hrnjić for the preparation of modified floating electrode schemes. We would like to thank the Slovenian research agency (ARRS) programs P2-0393 and P2-0084; the projects N2-0106, NC-0016, N2-0155 and N2-0248; NATO Science for Peace and Security Program under grant G5729; and European Research Council (ERC) Starting Grant 123STABLE (Grant agreement ID: 852208) for funding the study. A.R.K. would like to acknowledge the Janko Jamnik Doctoral Scholarship.

Supplementary materials

Supplementary material associated with this article can be found, in the online version, at doi:10.1016/j.electacta.2022.140800.

References

[1] C. Minke, M. Suermann, B. Bensmann, R. Hanke-Rauschenbach, Is iridium demand a potential bottleneck in the realization of large-scale PEM water electrolysis? Int. J. Hydrogen Energy 46 (2021) 23581–23590, https://doi.org/10.1016/j.ijhydene.2021.04.174.

[2] M. Bernt, A. Siebel, H.A. Gasteiger, Analysis of voltage losses in PEM water electrolyzers with low platinum group metal loadings, J. Electrochem. Soc. 165 (2018) F305–F314, https://doi.org/10.1149/2.0641805jes.

[3] G.S. Harzer, J.N. Schwämmlein, A.M. Damjanović, S. Ghosh, H.A. Gasteiger, Cathode loading impact on voltage cycling induced PEMFC degradation: a voltage loss analysis, J. Electrochem. Soc. 165 (2018) F3118–F3131, https://doi.org/10.1149/2.0161806jes.

[4] V.K. Puthiyapura, S. Pasupathi, H. Su, X. Liu, B. Pollet, K. Scott, Investigation of supported IrO2 as electrocatalyst for the oxygen evolution reaction in proton exchange membrane water electrolyser, Int. J. Hydrogen Energy 39 (2014) 1905–1913, https://doi.org/10.1016/j.ijhydene.2013.11.056.

[5] M. Ledendecker, S. Geiger, K. Hengge, J. Lim, S. Cherevko, A.M. Mingers, D. Göhl, G.V. Fortunato, D. Jalalpoor, F. Schüth, C. Scheu, K.J.J. Mayrhofer, Towards maximized utilization of iridium for the acidic oxygen evolution reaction, Nano Res. 12 (2019) 2275–2280, https://doi.org/10.1007/s12274-019-2383-y.

[6] H. Ohno, S. Nohara, K. Kakinuma, M. Uchida, H. Uchida, Effect of electronic conductivities of iridium oxide/doped SnO2 oxygen-evolving catalysts on the polarization properties in proton exchange membrane water electrolysis, Catalysts 9 (2019) 5–7, https://doi.org/10.3390/catal9010074.

[7] C. Van Pham, M. Bühler, J. Knöppel, M. Bierling, D. Seeberger, D. Escalera-López, K.J.J. Mayrhofer, S. Cherevko, S. Thiele, IrO2 coated TiO2 core-shell microparticles advance performance of low loading proton exchange membrane water electrolyzers, Appl. Catal. B Environ. 269 (2020), 118762, https://doi.org/10.1016/j.apcatb.2020.118762.

[8] E. Oakton, D. Lebedev, M. Povia, D.F. Abbott, E. Fabbri, A. Fedorov, M. Nachtegaal, C. Copéret, T.J. Schmidt, IrO2-TiO2: a high-surface-area, active, and stable electrocatalyst for the oxygen evolution reaction, ACS Catal. 7 (2017) 2346–2352, https://doi.org/10.1021/acscatal.6b03246.

[9] L. Wang, P. Lettenmeier, U. Golla-Schindler, P. Gazdzicki, N.A. Cañas, T. Morawietz, R. Hiesgen, S.S. Hosseiny, A.S. Gago, K.A. Friedrich, Nanostructured Ir-supported on Ti4O7 as a cost-effective anode for proton exchange membrane (PEM) electrolyzers, Phys. Chem. Chem. Phys. 18 (2016) 4487–4495, https://doi.org/10.1039/c5cp05296c.

[10] M. Bele, K. Stojanovski, P. Jovanovič, L. Moriau, G. Koderman Podboršek, J. Moškon, P. Umek, M. Sluban, G. Dražič, N. Hodnik, M. Gaberšček, Towards stable and conductive titanium oxynitride high-surface-area support for iridium nanoparticles as oxygen evolution reaction electrocatalyst, ChemCatChem 11 (2019) 5038–5044, https://doi.org/10.1002/cctc.201901487.

[11] B. Han, M. Risch, S. Belden, S. Lee, D. Bayer, E. Mutoro, Y. Shao-Horn, Screening oxide support materials for OER catalysts in acid, J. Electrochem. Soc. 165 (2018) F813–F820, https://doi.org/10.1149/2.0921810jes.

[12] S. Geiger, O. Kasian, A.M. Mingers, K.J.J. Mayrhofer, S. Cherevko, Stability limits of tin-based electrocatalyst supports, Sci. Rep. 7 (2017) 1–7, https://doi.org/10.1038/s41598-017-04079-9.

[13] L. Wang, F. Song, G. Ozouf, D. Geiger, T. Morawietz, M. Handl, P. Gazdzicki, C. Beauger, U. Kaiser, R. Hiesgen, A.S. Gago, K.A. Friedrich, Improving the activity and stability of Ir catalysts for PEM electrolyzer anodes by SnO2:Sb aerogel supports: does V addition play an active role in electrocatalysis? J. Mater. Chem. A 5 (2017) 3172–3178, https://doi.org/10.1039/c7ta00679a.

[14] K. Chen, T. Shen, Y. Lu, Y. Hu, J. Wang, J. Zhang, D. Wang, Engineering titanium oxide-based support for electrocatalysis, J. Energy Chem. 67 (2022) 168–183, https://doi.org/10.1016/j.jechem.2021.09.048.

[15] C.T. Campbell, Catalyst-support interactions: Electronic perturbations, Nat. Chem. 4 (2012) 597–598, https://doi.org/10.1038/nchem.1412.

[16] J.C. Matsubu, S. Zhang, L. DeRita, N.S. Marinkovic, J.G. Chen, G.W. Graham, X. Pan, P. Christopher, Adsorbate-mediated strong metal-support interactions in oxide-supported Rh catalysts, Nat. Chem. 9 (2017) 120–127, https://doi.org/10.1038/NCHEM.2607.

[17] A.R. Puigdollers, P. Schlexer, S. Tosoni, G. Pacchioni, Increasing oxide reducibility: the role of metal/oxide interfaces in the formation of oxygen vacancies, ACS Catal. 7 (2017) 6493–6513, https://doi.org/10.1021/acscatal.7b01913.

[18] A. Bruix, J.A. Rodriguez, P.J. Ramírez, S.D. Senanayake, J. Evans, J.B. Park, D. Stacchiola, P. Liu, J. Hrbek, F. Illas, A new type of strong metal–support interaction and the production of H2 through the transformation of water on Pt/CeO2 (111) and Pt/CeOx/TiO2 (110) catalysts, J. Am. Chem. Soc. 134 (2012) 8968–8974, https://doi.org/10.1021/ja302070k.

[19] S.J. Tauster, Strong metal-support interactions, Acc. Chem. Res. 20 (1987) 389–394, https://doi.org/10.1021/ar00143a001.

[20] H.S. Oh, H.N. Nong, T. Reier, A. Bergmann, M. Gliech, J. Ferreira De Araújo, E. Willinger, R. Schlögl, D. Teschner, P. Strasser, Electrochemical catalyst-support effects and their stabilizing role for IrOx nanoparticle catalysts during the oxygen evolution reaction, J. Am. Chem. Soc. 138 (2016) 12552–12563, https://doi.org/10.1021/jacs.6b07199.

[21] M. Bele, P. Jovanovič, Ž. Marinko, S. Drev, V.S. Šelih, J. Kovač, M. Gaberščcek, G. Koderman Podboršek, G. Dražić, N. Hodnik, A. Kokalj, L. Suhadolnik, Increasing the oxygen-evolution reaction performance of nanotubular titanium oxynitride-supported Ir nanoparticles by a strong metal–support interaction, ACS Catal. 10 (2020) 13688–13700, https://doi.org/10.1021/acscatal.0c03688.

[22] V.A. Saveleva, L. Wang, O. Kasian, M. Batuk, J. Hadermann, J.J. Gallet, F. Bournel, N. Alonso-Vante, G. Ozouf, C. Beauger, K.J.J. Mayrhofer, S. Cherevko, A.S. Gago, K.A. Friedrich, S. Zafeiratos, E.R. Savinova, Insight into the mechanisms of high activity and stability of iridium supported on antimony-doped tin oxide aerogel for anodes of proton exchange membrane water electrolyzers, ACS Catal. 10 (2020) 2508–2516, https://doi.org/10.1021/acscatal.9b04449.

[23] O. Kasian, J.P. Grote, S. Geiger, S. Cherevko, K.J.J. Mayrhofer, The common intermediates of oxygen evolution and dissolution reactions during water electrolysis on iridium, Angew. Chem. 57 (2018) 2488–2491, https://doi.org/10.1002/anie.201709652.

[24] N. Hodnik, S. Cherevko, Spot the difference at the nanoscale: identical location electron microscopy in electrocatalysis, Curr. Opin. Electrochem. 15 (2019) 73–82, https://doi.org/10.1016/j.coelec.2019.03.007.

[25] M. Arenz, A. Zana, Fuel cell catalyst degradation: Identical location electron microscopy and related methods, Nano Energy 29 (2016) 299–313, https://doi.org/10.1016/j.nanoen.2016.04.027.

[26] J. Aarons, L. Jones, A. Varambhia, K.E. MacArthur, D. Ozkaya, M. Sarwar, C. K. Skylaris, P.D. Nellist, Predicting the oxygen-binding properties of platinum nanoparticle ensembles by combining high-precision electron microscopy and density functional theory, Nano Lett. 17 (2017) 4003–4012, https://doi.org/10.1021/acs.nanolett.6b04799.

[27] L.J. Moriau, A. Hrnjić, A. Pavlišič, A.R. Kamšek, U. Petek, F. Ruiz-Zepeda, M. Šala, L. Pavko, V.S. Šelih, M. Bele, P. Jovanovič, M. Gatalo, N. Hodnik, Resolving the nanoparticles' structure-property relationships at the atomic level: a study of Pt-based electrocatalysts, IScience 24 (2021), 102102, https://doi.org/10.1016/j.isci.2021.102102.

[28] A. Hrnjić, F. Ruiz-Zepeda, M. Gaberščcek, M. Bele, L. Suhadolnik, N. Hodnik, P. Jovanovič, Modified floating electrode apparatus for advanced characterization of oxygen reduction reaction electrocatalysts, J. Electrochem. Soc. 167 (2020), 166501, https://doi.org/10.1149/1945-7111/abc9de.

[29] M. Fathi Tovini, A. Hartig-Weiß, H.A. Gasteiger, H.A. El-Sayed, The discrepancy in oxygen evolution reaction catalyst lifetime explained: RDE vs MEA - dynamicity within the catalyst layer matters, J. Electrochem. Soc. 168 (2021), 014512, https://doi.org/10.1149/1945-7111/abdcc9.

[30] H.A. El-Sayed, A. Weiß, L.F. Olbrich, G.P. Putro, H.A. Gasteiger, OER catalyst stability investigation using RDE technique: a stability measure or an artifact? J. Electrochem. Soc. 166 (2019) F458–F464, https://doi.org/10.1149/2.0301908jes.

[31] P. Jovanovič, K. Stojanovski, M. Bele, G. Dražić, G. Koderman Podboršek, L. Suhadolnik, M. Gaberščcek, N. Hodnik, Methodology for investigating electrochemical gas evolution reactions: floating electrode as a means for effective gas bubble removal, Anal. Chem. 91 (2019) 10353–10356, https://doi.org/10.1021/acs.analchem.9b01317.

[32] A. Hrnjic, A.R. Kamšek, A. Pavlišič, M. Šala, M. Bele, L. Moriau, M. Gatalo, F. Ruiz-Zepeda, P. Jovanovič, N. Hodnik, Observing, tracking and analysing electrochemically induced atomic-scale structural changes of an individual Pt-Co nanoparticle as a fuel cell electrocatalyst by combining modified floating electrode and identical location electron microscopy, Electrochim. Acta 388 (2021), 138513, https://doi.org/10.1016/j.electacta.2021.138513.

[33] N. Hodnik, C. Baldizzone, G. Polymeros, S. Geiger, J.-P. Grote, S. Cherevko, A. Mingers, A. Zeradjanin, K.J.J. Mayrhofer, Platinum recycling going green via induced surface potential alteration enabling fast and efficient dissolution, Nat. Commun. 7 (2016) 13164, https://doi.org/10.1038/ncomms13164.

[34] M.K. Jha, J.C. Lee, M.S. Kim, J. Jeong, B.S. Kim, V. Kumar, Hydrometallurgical recovery/recycling of platinum by the leaching of spent catalysts: a review, Hydrometallurgy 133 (2013) 23–32, https://doi.org/10.1016/j.hydromet.2012.11.012.

[35] I. Yakoumis, M. Panou, A.M. Moschovi, D. Panias, Recovery of platinum group metals from spent automotive catalysts: a review, Clean. Eng. Technol. 3 (2021), 100112, https://doi.org/10.1016/j.clet.2021.100112.

[36] L. Moriau, M. Bele, Ž. Marinko, F. Ruiz-Zepeda, G. Koderman Podboršek, M. Šala, A.K. Šurca, J. Kovač, I. Arčon, P. Jovanovič, N. Hodnik, L. Suhadolnik, Effect of the morphology of the high-surface-area support on the performance of the oxygen-evolution reaction for iridium nanoparticles, ACS Catal. 11 (2021) 670–681, https://doi.org/10.1021/acscatal.0c04741.

[37] Y.R. Zheng, J. Vernieres, Z. Wang, K. Zhang, D. Hochfilzer, K. Krempl, T.W. Liao, F. Presel, T. Altantzis, J. Fatermans, S.B. Scott, N.M. Secher, C. Moon, P. Liu, S. Bals, S. Van Aert, A. Cao, M. Anand, J.K. Nørskov, J. Kibsgaard, I. Chorkendorff, Monitoring oxygen production on mass-selected iridium–tantalum oxide electrocatalysts, Nat. Energy (2021), https://doi.org/10.1038/s41560-021-00948-w.

[38] C. Wei, S. Sun, D. Mandler, X. Wang, S.Z. Qiao, Z.J. Xu, Approaches for measuring the surface areas of metal oxide electrocatalysts for determining their intrinsic electrocatalytic activity, Chem. Soc. Rev. 48 (2019) 2518–2534, https://doi.org/10.1039/c8cs00848e.

[39] S. Watzele, P. Hauenstein, Y. Liang, S. Xue, J. Fichtner, B. Garlyyev, D. Scieszka, F. Claudel, F. Maillard, A.S. Bandarenka, Determination of electroactive surface area of Ni-, Co-, Fe-, and Ir-based oxide electrocatalysts, ACS Catal. 9 (2019) 9222–9230, https://doi.org/10.1021/acscatal.9b02006.

[40] C. Wei, S. Sun, D. Mandler, X. Wang, S.Z. Qiao, Z.J. Xu, Approaches for measuring the surface areas of metal oxide electrocatalysts for determining their intrinsic electrocatalytic activity, Chem. Soc. Rev. 48 (2019) 2518–2534, https://doi.org/10.1039/c8cs00848e.

[41] S. Cherevko, S. Geiger, O. Kasian, A. Mingers, K.J.J. Mayrhofer, Oxygen evolution activity and stability of iridium in acidic media. Part 1. - Metallic iridium, J. Electroanal. Chem. 773 (2016) 69–78, https://doi.org/10.1016/j.jelechem.2016.04.033.

[42] A. Weiß, A. Siebel, M. Bernt, T.-H. Shen, V. Tileli, H.A. Gasteiger, Impact of intermittent operation on lifetime and performance of a PEM Water electrolyzer, J. Electrochem. Soc. 166 (2019) F487–F497, https://doi.org/10.1149/2.0421908jes.

[43] S. Czioska, A. Boubnov, D. Escalera-López, J. Geppert, A. Zagalskaya, P. Röse, E. Saraçi, V. Alexandrov, U. Krewer, S. Cherevko, J.-D. Grunwaldt, Increased Ir–Ir interaction in iridium oxide during the oxygen evolution reaction at high potentials probed by operando spectroscopy, ACS Catal. 11 (2021) 10043–10057, https://doi.org/10.1021/acscatal.1c02074.

[44] R. Woods, Hydrogen adsorption on platinum, iridium and rhodium electrodes at reduced temperatures and the determination of real surface area, J. Electroanal. Chem. 49 (1974) 217–226, https://doi.org/10.1016/S0022-0728(74)80229-9.

[45] T. Li, O. Kasian, S. Cherevko, S. Zhang, S. Geiger, C. Scheu, P. Felfer, D. Raabe, B. Gault, K.J.J. Mayrhofer, Atomic-scale insights into surface species of electrocatalysts in three dimensions (SI), Nat. Catal. 1 (2018) 300–305, https://doi.org/10.1038/s41929-018-0043-3.

[46] E. Özer, C. Spöri, T. Reier, P. Strasser, Iridium(1 1 1), iridium(1 1 0), and ruthenium(0 0 0 1) single crystals as model catalysts for the oxygen evolution reaction: insights into the electrochemical oxide formation and electrocatalytic activity, ChemCatChem 9 (2017) 597–603, https://doi.org/10.1002/cctc.201600423.

[47] M. Scohy, S. Abbou, V. Martin, B. Gilles, E. Sibert, L. Dubau, F. Maillard, Probing surface oxide formation and dissolution on/of Ir single crystals via X-ray photoelectron spectroscopy and inductively coupled plasma mass spectrometry, ACS Catal. 9 (2019) 9859–9869, https://doi.org/10.1021/acscatal.9b02988.

[48] A. BalaKrishnan, N. Blanc, U. Hagemann, P. Gemagami, K. Wonner, K. Tschulik, T. Li, Direct detection of surface species formed on iridium electrocatalysts during the oxygen evolution reaction, Angew. Chem. 133 (2021) 21566–21573, https://doi.org/10.1002/ange.202106790.

[49] P.G. Pickup, V.I. Birss, A model for anodic hydrous oxide growth at iridium, J. Electroanal. Chem. 220 (1987) 83–100, https://doi.org/10.1016/0022-0728(87)88006-3.

[50] S. Cherevko, S. Geiger, O. Kasian, A. Mingers, K.J.J. Mayrhofer, Oxygen evolution activity and stability of iridium in acidic media. Part 2. - electrochemically grown hydrous iridium oxide, J. Electroanal. Chem. 774 (2016) 102–110, https://doi.org/10.1016/j.jelechem.2016.05.015.

[51] A. Lončar, D. Escalera-López, F. Ruiz-Zepeda, A. Hrnjić, M. Šala, P. Jovanovič, M. Bele, S. Cherevko, N. Hodnik, Sacrificial Cu layer mediated the formation of an active and stable supported iridium oxygen evolution reaction electrocatalyst, ACS Catal. 11 (2021) 12510–12519, https://doi.org/10.1021/acscatal.1c02968.

[52] Z. Pavlovic, C. Ranjan, Q. Gao, M. Van Gastel, R. Schlögl, Probing the structure of a water-oxidizing anodic iridium oxide catalyst using raman spectroscopy, ACS Catal. 6 (2016) 0–7, https://doi.org/10.1021/acscatal.6b02343.

[53] H. An, L. Wu, L.D.B. Mandemaker, S. Yang, J. de Ruiter, J.H.J. Wijten, J.C. L. Janssens, T. Hartman, W. van der Stam, B.M. Weckhuysen, Sub-second time-resolved surface-enhanced raman spectroscopy reveals dynamic CO intermediates during electrochemical CO2 reduction on copper, Angew. Chem. 60 (2021) 16576–16584, https://doi.org/10.1002/anie.202104114.